Photodetected Power Maximization of Photonically Generated Impulse Radio Ultrawide Band Signals

Mohamed Shehata[1], Mohamed Sameh Said[1], and Hassan Mostafa[1,2]
[1]Electronics and Electrical Communications Engineering Department, Cairo University, Giza 12613, Egypt
[2]Nanotechnolgy Department at Zewail City of Science and Technology, Giza, Egypt
Emails: [1]m.shehata_ieee@yahoo.com, [2]msmsab@hotmail.com, [3]hmostafa@uwaterloo.ca

***Abstract*—Microwave photonic (MWP) processing of impulse radio ultra wideband (IR-UWB) waveforms is the most critical stage in IR-UWB over fiber (IR-UWBoF) systems with optical and/or wireless transmission. In these systems, a centralized optical processing hub is the only place where a power efficient IR-UWB signal can be generated prior to optical distribution to an optical-wireless interface. In this work, very accurate analytical expressions for the photodetected optical power of photonically generated IR-UWB waveforms are derived and maximized, considering two common types of IR-UWB waveforms. Numerical simulations show excellent agreement with the obtained analytical expressions and provide useful design insights as well as guidelines in the development of IR-UWBoF systems.**

***Index Terms*—Impulse radio(IR), microwave photonic (MWP), ultra wideband over fiber (UWBoF).**

I. Introduction

The increasing public demands on clustered indoor wireless access services has directed much of the research efforts to short range wireless technologies that possess a high spatio-spectral throughput. The main challenge has been the frequency allocation of new standards in a congested radio spectrum. In 2002, the US Federal Communications Committee (FCC) has licensed the use of the entire radio spectrum for UWB signalling under extremely low power spectral density (PSD) constraints that does not exceed -41.3 dBm/MHz to avoid destructive interference with previously standardized wireless services [1]. These PSD constraints have limited the applications of UWB signalling to the desired clustered high speed indoor communications scenarios as the limited effective isotropic radiated power (ERIP) of these signals does not support their propagation for more than 4-10 m.

However, the under-utilized spatial throughput offered by the UWB technology has promoted the optical distribution of UWB signals over optical fibers to geographically remote locations, where the excess UWB capacity can be utilized by remotely located users. Photonic generation of IR-UWB signals by electro-optic conversion has been a natural solution, emerging in a hybrid IR-UWB over fiber (IR-UWBoF) transceiver chain [2]. However, the selective frequency response of IR-UWBoF links tend to suppress their received PSD as well as their photodetected power at the electrical receiver front end. Since the photodetected IR-UWB signal power depends on the spectrum of the particular IR-UWB signalling waveform as well as the IR-UWBoF systems parameters, the spectrum of an IR-UWB waveform should be carefully shaped in order to achieve the highest received power and a minimum BER at the ultimate user end in an IR-UWBoF link [3]. Most often, IR-UWB waveform photonic generation techniques aim at producing power efficient IR-UWB waveforms from amplitude and/or time derivatives of Gaussian [4] and sech [5] pulses. However, due to the numerous possibilities of implementing IR-UWBoF system using the various optical phenomena, exhibited by optical devices, it has become a common practice to optimize the performance of photonic generation techniques by roughly adjusting their design parameters. Generally, according to [6], radio over fiber (RoF) systems, formed by merely connecting optimally operating standalone optical components, do not necessarily show optimal performance. To the best of the authors' knowledge, no analytical expressions have been reported to model the average photodetected power of the photonically generated IR-UWB waveforms in IR-UWBoF systems. In this paper, an elegant approach is introduced to calculate and maximize the average photodetected power of these two waveform types.

The rest of this paper is organized as follows. First, a typical IR-UWB waveform electro-optic conversion technique is described and modelled in Section (II). In Section (III), analytical expressions for the average received photodetected power of both waveform types are developed. The obtained expressions are then numerically evaluated, maximized and analyzed in Section (V). Based on the obtained results, the whole paper is finally concluded in Section (IV).

II. System Model Overview

Fig.1 depicts the schematic diagram of a typical IR-UWB waveform photonic generation technique, inspired from the general circuit model of RoF systems provided in [6]. It consists of a continuous wave (CW) laser diode (LD), whose output optical power is controlled via a variable optical attenuator (VOA), a Mach-Zhender modulator (MZM), a standard single mode fiber (SSMF) and a high speed photodetector (PD). The wireless transmission chain, following the PD, is modelled by an equivalent load resistance R_L, where the photodetected power of an IR-UWB signal is transferred. A stream of independent and identically distributed (i.d.d) binary encoded waveforms, emitted by an information source, is applied to the radio frequency (RF) input port of the MZM,

978-1-5386-4881-0/18/$31.00 ©2018 IEEE

while the output of the LD is applied to the optical input port of the MZM. A DC voltage of V_B is applied to the bias port of the MZM. The complex envelope of the optical electrical field at the MZM-optical fiber interface is given by

$$E(t) = \sqrt{2P_o}\exp(j2\pi c/\lambda_o) \times \left\{\exp\left(j\frac{\beta}{2}w(t) \pm j\frac{\pi}{2}\right) + \exp\left(-j\frac{\beta}{2}w(t)\right)\right\} \quad (1)$$

where P_o is the optical power emitted by the LD, λ_o is the wavelength of the optical CW, β is the phase modulation index of the MZM, measured in rad/V and $w(t)$ is an electrical replica of the optical IR-UWB waveform. The $\pm$ sign accounts for the two possibilities of the 1 and 0 bits, respectively. The electric IR-UWB waveform $w(t)$ in (1) is given by $\psi^{(m)}(t,\tau) = d^m\psi(t,\tau)/dt^m; t \in \mathbf{R}$, where $\psi(t,\tau)$ is an IR-UWB basis function and τ is its temporal pulse shaping factor. This input basis function is given by either an amplitude normalized Gaussian pulse which is typically expressed as $\psi(t,\tau) = \exp(-t^2/{\tau_g}^2)$, where τ_g is the Gaussian pulse width or an amplitude normalized sech pulse which is typically expressed as $\psi(t,\tau) = \mathrm{sech}(t/\tau_s)$, where τ_s is the sech pulse width. The pulse shaping factor of $\psi(t,\tau)$ is defined as its full width at half maximum (FWHM) pulse width and is related to the Gaussian and sech pulse widths as $\tau_g \triangleq \tau/2\sqrt{\log(2)}$ and $\tau_s \triangleq \tau/2\mathrm{sech}^{-1}(0.5)$, respectively. At the MZM output, the encoded optical waveforms are propagated down an L km length of the SSMF to a remote location, where the PD is located. Generally, the complex baseband frequency domain transfer function of a SSMF is expressed, in terms of its Taylor series expansion, as [7]:

$$H_{SSMF}(j\omega) = H_o\exp\left(-j\sum_{n=0}^{\infty}\frac{k_nL}{n!}(\omega - 2\pi c/\lambda_o)^n\right) \quad (2)$$

where $H_o = \exp(-\alpha L)$ is a constant that accounts for the fiber loss, α is the fiber attenuation constant, usually measured in dB/km, L is the optical fiber length, k_n is n^{th} order propagation constant of the SSMF and $c = 3\times10^8 m/s$ is the speed of light.

The optical waveform at the output end of the SSMF is applied to the high speed photo-detector (PD) for purpose of optical-to-electrical conversion such that the desired temporal electrical IR-UWB waveform is obtained. The power of the photodetected IR-UWB waveform depends on the attenuation, the n^{th} order dispersion coefficient, k_n as well as the length of the SSMF. However, a short (e.g., less than 1 km) length SSMF is assumed, such that the dispersion has negligible effects on the link performance and only the attenuation loss H_o. is considered. The optical electric field at output end of the optical fiber is applied to a high speed PD for square law detection. The photocurrent at the PD output is expressed as follows:

$$I_{PD}(t) = \Re\sqrt{2P_o}H_o\left(1 \mp \sin\left(\beta\psi^{(m)}(t,\tau)\right)\right) \quad (3)$$

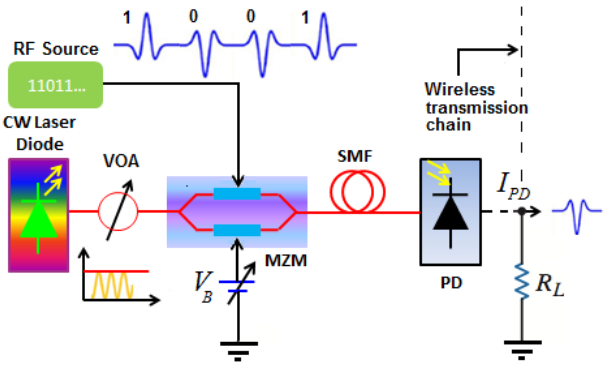

Fig. 1. Block diagram of a typical IR-UWBoF communication system. Red lines : optical paths. Black lines : electrical paths.

Clearly, the desired part of the photodetected IR-UWB signal power is expressed in terms of the AC component of the photocurrent in (3). Assuming small signal biasing condition for the MZM, corresponding to $\beta \leq \pi/6$, the photocurrent in (3) becomes:

$$I_{PD}(t) \approx \Re\sqrt{2P_o}H_o\psi^{(m)}(t,\tau) \quad (4)$$

Applying Parseval's theorem, the average photodetected power of the IR-UWB signal is given by

$$\overline{P}_{PD} = \int_{-\infty}^{+\infty}\left|A^m\Psi^{(m)}(j\omega,\tau)\right|^2 d\omega \quad (5)$$

where $A^m \triangleq \sqrt{P_o}\Re R_L\beta H_o/\sqrt{2}\pi$ is the amplitude of the m^{th} order IR-UWB waveform, $\Psi^{(m)}(j\omega,\tau) = \Im\{\psi^{(m)}(t,\tau)\}$ is the Fourier transform of $\psi^{(m)}(t,\tau)$, ω is the angular frequency and $\Im\{.\}$ denotes the Fourier transform operation.

III. Photodetected Power Maximization

Fig. 2 plots the FCC PSD constrains on UWB signals. Although small, a maximum admissible PSD of -41.3 dBm/MHz is allowed over a huge bandwidth of 7.5 GHz, usually called the useful UWB band, ranging from 3.1 GHz to 10.6 GHz. Accordingly, two conditions should be satisfied to efficiently utilize this huge bandwidth and achieve a high signalling rate under the FCC spectral constraints. Firstly, A^m should be adjusted such that the maximum PSD of the UWB signal does not exceed the maximum PSD admissible by the FCC. Secondly, the bandwidth of the UWB signal should be located within the useful UWB band. In particular, A^m is defined as follows:

$$A^m \triangleq \left(\max\left\{S_{FCC}(\omega)\right\} / \max\left\{\left|\Psi^{(m)}(\omega,\tau)\right|^2\right\}\right)^{1/2} \quad (6)$$

where $S_{FCC}(\omega)$ is the maximum PSD admissible by the FCC mask within the useful UWB band. The amplitude normalized Fourier transform of the m^{th} order Gaussian-based derivative is given by

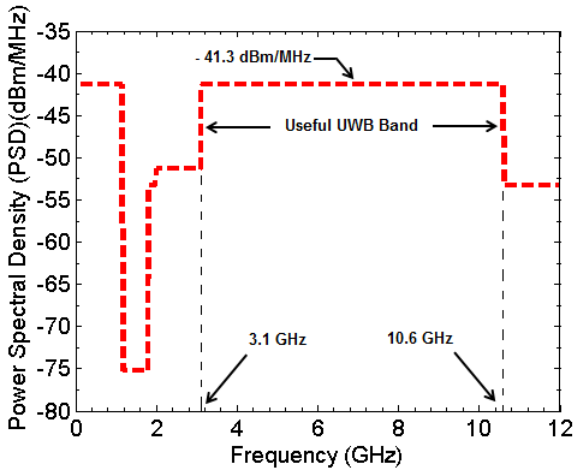

Fig. 2. The spectral constraints of the FCC mask.

$$\Psi^{(m)}_{n,FCC}(\omega,\tau) = A^m_g (j\omega)^m \tau_g \sqrt{\pi} \exp(-(\omega\tau_g)^2/2) \quad (7)$$

whereas the amplitude normalized Fourier transform of the m^{th} order sech-based derivative, $\Psi^{(m)}_{n,FCC}(\omega,\tau)$ is given by

$$\Psi^{(m)}_{n,FCC}(\omega,\tau) = A^m_s (j\omega)^m 4\pi\tau_s \text{sech}(2\pi\omega\tau_s) \quad (8)$$

In what follows, $\Psi^{(m)}_{n,FCC}(\omega,\tau)$ refers to one of the definitions (7) or (8) as required. Since Gaussian and sech-based derivatives are characterized by a unique global maximum, the value of ω that leads to $\left|\Psi^{(m)}(\omega,\tau)\right|^2 = \max\left\{\left|\Psi^{(m)}(\omega,\tau)\right|^2\right\}$ is obtained by substituting either of the definitions (7) or (8) in $\partial\left|\Psi^{(m)}_{n,FCC}(\omega,\tau)\right|^2/\partial\omega = 0$ and solving for ω . The result is defined as the peak emission angular frequency, denoted by $\omega_{p,g}$ for Gaussian-based waveforms and $\omega_{p,s}$ for sech-based waveforms. The values of A^m_g and A^m_s are obtained by substituting $\omega_{p,g}$ and $\omega_{p,s}$ in (6) as follows:

$$A^m_g = \left(S_{FCC}(\omega)/\omega^{2m}_{p,g}\pi\tau^2_g \exp\left(-(\omega_{p,g}\tau_g)^2/2\right)\right)^{1/2} \quad (9)$$

$$A^m_s = \left(S_{FCC}(\omega)/\omega^{2m}_{p,s}(4\pi\tau_s)^2 \text{sech}^2\left(2\pi\omega_{p,s}\tau_s\right)\right)^{1/2} \quad (10)$$

Since most of the PSD of the IR-UWB signal is concentrated in the useful UWB band, the photodetected power in (5) can be approximated as follows:

$$\overline{P}_{PD} = \int_{-\infty}^{\infty} |\Psi^{(m)}_{n,FCC}(j\omega,\tau)| d\omega \approx 2\int_{\omega_L}^{\omega_H} |\Psi^{(m)}_{n,FCC}(j\omega,\tau) d\omega \quad (11)$$

The power of Gaussian-based IR-UWB waveforms at the PD output is analytically obtained by substituting (7) in (11) as follows:

$$\begin{aligned}\overline{P}_{PD,g}(\tau_g) &= \pi(\tau_g A^m_g)^2 \int_{\omega_L}^{\omega_H} \omega^m \exp\left(-(\omega\tau_g)^2\right) d\omega \\ &= G_p \times \left(\Xi(\omega_H\tau_g/\sqrt{2}) - \Xi(\omega_L\tau_g/\sqrt{2})\right)\end{aligned} \quad (12)$$

where $G_p = 2\pi(\tau_g A^m_g)^2\left(\sqrt{2}/\tau_g\right)^{m+1}$, A^m_g is the normalization constant of the m^{th} order derivative of a Gaussian-based IR-UWB waveform and $\Xi(u)$ is given by

$$\begin{aligned}\Xi(u) &= (1-s)\Gamma\left(\frac{m+s+1}{2}\right)\left(1-2Q(\sqrt{2}u)\right) \\ &- \exp(-u^2)\sum_{n=0}^{L-1}\frac{\Gamma(\frac{m+1}{2})}{\Gamma(\frac{m+1}{2}-n)}u^{m-2n-1}\end{aligned} \quad (13)$$

with $s = (m+1) \bmod 2$, $L = (m+s)/2, \Gamma(z)$ and $Q(u)$ are the conventional Gamma function and the conventional Gaussian Q-function, defined as $Q(u) = (1/\sqrt{2\pi})\int_y^{\infty}\exp(-y^2)dy$ and $\Gamma(z) = \int_{x=0}^{\infty} y^{z-1}\exp(-y)dy$, respectively. Similarly, the photodetected power is analytically obtained for sech-based IR-UWB waveforms by substituting (8) in (11) as follows:

$$\begin{aligned}\overline{P}_{PD,s}(\tau_s) &= 2(A^m_s)^2 \int_{\omega_L}^{\omega_H} \omega^m (4\pi\tau_s)^2 \text{sech}^2\left(2\pi\omega\tau_s\right) d\omega \\ &= S_p \times \left(\Lambda(2\pi\omega_H\tau_s) - \Lambda(2\pi\omega_L\tau_s)\right)\end{aligned} \quad (14)$$

where $S_p = 8m!(4\pi\tau_s A^m_s)^2(1/2\pi\tau_s)^{m+1}$, A^m_s is the normalization constant of the m^{th} order derivative of a sech-based IR-UWB waveform and $\Lambda(u)$ is given by

$$\begin{aligned}\Lambda(u) &= \sum_{l=0}^{K}\sum_{q=0}^{m}\frac{(-1)^{l+q}(l+1)}{(m-q)!(-2(l+1))^{q+1}} \\ &\times u^{m-q}\exp\left(-2(l+1)u\right); K \gg 4\end{aligned} \quad (15)$$

The higher the value of K is, the more accurate value of $\Lambda(u)$ is obtained. It should noted that, the analytical expressions in (12) and (14) constitute the upper bounds for the received power of the considered IR-UWB waveforms

IV. Simulation Results and Analysis

In this section, the average optical power expressions in (12) and (14) are numerically evaluated and optimized with respect to the FWHM pulse width τ over the range from 0 to 300 ps for Gaussian-based IR-UWB waveforms and from 0 up to 200 ps for sech-based IR-UWB waveforms. The first seven order derivatives of both waveform types are considered. The simulation starts by evaluating the values of $(\tau_g, A^m_g, \omega_{p,g})$ and $(\tau_s, A^m_s, \omega_{p,s})$ numerically. Based on the derived expression in (12), Fig.2 shows the variation of the average photodetected power with τ for Gaussian-based IR-UWB waveforms at different values of m. It can be observed that at a particular value of m, the average photodetected

978-1-5386-4881-0/18/$31.00 ©2018 IEEE

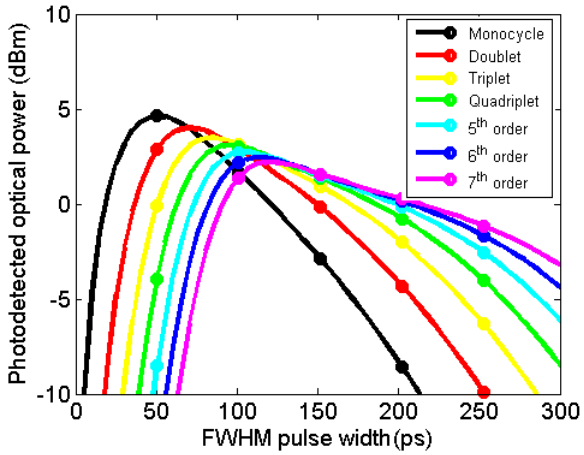

Fig. 3. Average photodetected optical power versus the FWHM pulse width of Gaussian-based IR-UWB waveforms. Solid lines: theoretically obtained results. Markers: Results obtained by numerical integration techniques.

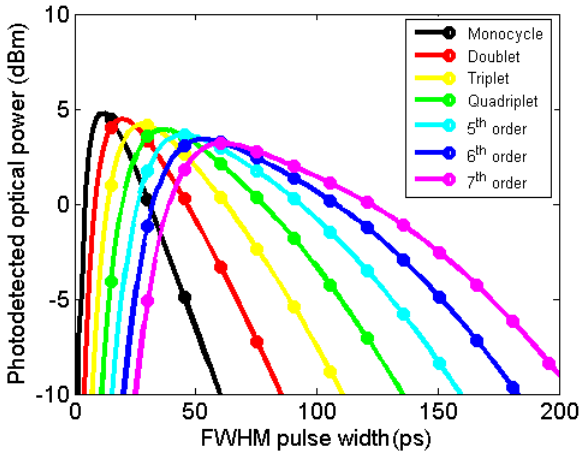

Fig. 4. Average photodetected optical power versus the FWHM pulse width of sech-based IR-UWB waveforms. Solid lines: theoretically obtained results. Markers: Results obtained by numerical integration techniques.

power increases monotonically from zero up to a maximum value with increasing τ from zero up to an optimum value where the average photodetected power attains its maximum. Further increase of τ leads to a degradation in the average photodetected power below its maximum value. For example, a Gaussian-based monocycle pulse having a FWHM pulse width of 50.51 ps achieves the maximum average photodetected power of 4.63 dBm. Gaussian-based doublets, triplets and higher order derivatives also show similar behaviour. However, the value of the optimum FWHM pulse width and the corresponding maximum attainable average photodetected power, decreases with increasing m. This can be interpreted as follows. Increasing the differentiation order m leads to shifting the UWB signal spectrum towards higher frequencies outside the window of the useful UWB band and less power is produced at the PD output. Likewise, Fig.3 presents the variation of the average photodetected power versus τ for sech-based IR-UWB waveforms according the expression derived in (14). The sech-based monocycle pulse achieves a maximum photodetected power value of 4.77 dBm at a FWHM input pulse width of 12.07 ps. Moreover, it is important to highlight that both Gaussian and sech-based monocycles outperforms doublets, triplets and higher order derivatives in terms of the highest achievable photodetected power. This observation supports the claims in [8] for preferring monocycle pulses in general, and sech-based monocycles in particular, as signalling waveforms in IR-UWB systems.

V. Conclusion

This paper presents accurate closed form expressions for the power photodetected power of a photonically generated IR-UWB waveform in centralized optical processing hybrid optical wireless systems. These expressions are derived, numerically evaluated and maximized under the FCC power spectral density constraints, considering two common IR-UWB waveform types. The derived expressions provide useful design guidelines for radio over fiber systems in general and IR-UWB over fiber systems in particular.

Acknowledgment

This work was funded by the national telecommunications regulatory authority (NTRA), Egypt and ONE (Opto-Nano-Electronics) Lab at Cairo University.

References

[1] US. Fed. Comm. Commission , First report and order, (Revision of part 15 of the commission's rules regarding ultra-wideband transmission systems),adopted Feb. 14, 2002, released Apr. 22, 2002. Tech. Rep.

[2] R. R. Lopez, A. Caballero, X. Yu, T. B. Gibbon, J. B. Jensen and I. T. Monroy, "A Comparison of Electrical and Photonic Pulse Generation for IR-UWB on Fiber Links," in IEEE Photonics Technology Letters, vol. 22, no. 5, pp. 263-265, March1, 2010.

[3] T. Wang, W. Heinzelman and A. Seyedi ,Link Energy Minimization in IR-UWB Based Wireless Networks, IEEE Transactions on Wireless Communications, vol. 9, no. 9, pp. 2800-2811, September, 2010.

[4] Qing Wang, Jianping Yao,Ultra-Wideband Gaussian monocycle and doublet pulse generation using a reconfigurable photonic microwave delay-line filter, in Radio and Wireless Symposium, 2008 IEEE , vol., no., pp.129-132, 22-24 Jan. 2008.

[5] M. Abtahi, M. Mirshafiei, S. LaRochelle and L. A. Rusch, "All-Optical 500-Mb/s UWB Transceiver:An Experimental Demonstration," in Journal of Lightwave Technology, vol. 26, no. 15, pp. 2795-2802, Aug.1, 2008.

[6] C. H. Cox, E. I. Ackerman, G. E. Betts and J. L. Prince, "Corrections to "Limits on the Performance of RF-Over-Fiber Links and Their Impact on Device Design"," in IEEE Transactions on Microwave Theory and Techniques, vol. 55, no. 2, pp. 351-351, Feb. 2007.

[7] H. Xia and J. Yao, "Characterization of Subpicosecond Pulses Based on Temporal Interferometry With Real-Time Tracking of Higher Order Dispersion and Optical Time Delay," in Journal of Lightwave Technology, vol. 27, no. 22, pp. 5029-5037, Nov.15, 2009.

[8] Shehata, M., Mostafa, H., and Ismail, Y. "Closed Form Expressions and Bounds for The Signal to Noise Ratio in IR-UWBoF Systems," *IEEE Photonics Technology Letters*, 29(6):507–510, March 2017.